Stability of heteroepitaxial coherent growth modes on nanowire radial surfaces

T. Riedl* and J. K. N. Lindner
Paderborn University, Department of Physics, Warburger Straße 100, 33098 Paderborn, Germany
and Center for Optoelectronics and Photonics Paderborn (CeOPP), Warburger Straße 100, 33098 Paderborn, Germany

(Received 22 August 2018; revised manuscript received 3 April 2019; published 28 May 2019)

The thermodynamic stability of the coherent shell and Stranski-Krastanov heteroepitaxial growth modes on cylindrical nanowires is analyzed theoretically. In contrast to previous studies, the exact geometrical shape of pyramidal Stranski-Krastanov islands is considered for the calculation of surface- and elastic-energy contributions. In particular, the impact of the pyramid base angle on the relaxation energy is included. Moreover, the dependence of island facet surface-energy density on the distance of the surface to the nanowire substrate is taken into account. Maps of the growth-mode stability are derived for the Si-core/Ge-shell structure, which display the favored mode as a function of deposited volume, wetting-layer thickness, and nanowire radius. We show that for nanowire radii in the range between 15 and 100 nm, the Stranski-Krastanov mode becomes stable only for larger pyramid angles. In addition, it is found that the exact value of the surface-energy density significantly influences the transition between the two growth modes, leading to a stabilization of islands bound by low-energy crystal facets, as observed in experiments.

DOI: 10.1103/PhysRevMaterials.3.053403

I. INTRODUCTION

Nanowire (NW) heterostructures comprise axial [1], radial [2,3], and branched [4,5] morphologies. For the fabrication vapor-liquid-solid or vapor-solid growth mechanisms using metal organic vapor phase epitaxy [6], molecular beam epitaxy [7,8] or chemical beam epitaxy [9] are widely employed. Also, atomic-layer deposition is used for the formation of NW shells [10,11]. On the radial surfaces of NWs, heteroepitaxial deposits usually grow in the form of a shell according to the Frank–van der Merwe (FM) mechanism or in the form of three-dimensional islands according to the Stranski-Krastanov (SK) mode [12]. Such NW radial heterostructures are of great interest for advanced optoelectronic devices such as lasers [13], light-emitting diodes [14,15], single-photon sources [16], field-effect transistors [2,17], or spintronics [18], as well as for fundamental studies of carrier confinement [19,20]. Heterostructured core-shell NWs exhibit outstanding electronic properties such as high carrier mobilities [17] and tunable band gaps [21].

Experimentally, for the Si-Ge system, core-shell growth is observed for small NW core diameters below 20 nm [2,12], whereas evidence for SK island growth is reported at larger diameters [12]. In order to understand the interplay between growth morphology and coherent strain relaxation in radial NW heterostructures, extensive theoretical and experimental studies have been performed, which address the occurrence, wavelength, and amplitude of strain-induced periodic perturbations on the growth surface [22–25]. The relative stability of the pure FM and SK growth modes has been predicted by thermodynamic approaches for the Si-Ge system [25,26]. Although these approaches take the self-relaxation of a misfit-strained cylindrical shell layer into account, they suffer from several restrictions and simplifications:

(i) The formula derived by Shchukin *et al.* [27] for the calculation of the SK island elastic relaxation energy and used by Li and Yang [26] implies a constant in-plane strain component as a function of the vertical coordinate (perpendicular to the NW axis) and therefore is restricted to flat islands of low aspect ratio.

(ii) For computation of the island volume as well as of the facet surface area and the NW surface area beneath the island, the influence of NW curvature is neglected.

(iii) Concerning the surface energy of the island facets the exponential dependence of the surface energy on the distance to the substrate interface [28] is neglected.

In the present study, we reanalyze the stability of the pure FM and SK growth modes in consideration of the actual volume and surface area of a pyramidal island on a cylindrical NW substrate as well as the distance dependence of the pyramid surface energy and the influence of the pyramid angle on the island relaxation energy. This improved model is outlined in Sec. II. Section III presents and discusses the results for the Si-Ge system. The approach can be transferred to other material systems as well. In Sec. IV, we draw conclusions. Details of the calculations are delineated in Appendices A and B.

II. GEOMETRIC-STRUCTURAL AND CONTINUUM ENERGY-DENSITY MODELING

In the following, we consider the growth of Ge on a single cylindrical Si NW covered with a preexisting Ge wetting layer (WL), either in the form of a homogeneous shell or SK islands, in an analogous manner as previously done by Li and Yang [26]. Let ΔE_{SK} and ΔE_{FM} be the change in the formation energy in the SK and FM growth mode, respectively, with

*Corresponding author: thomas.riedl@uni-paderborn.de

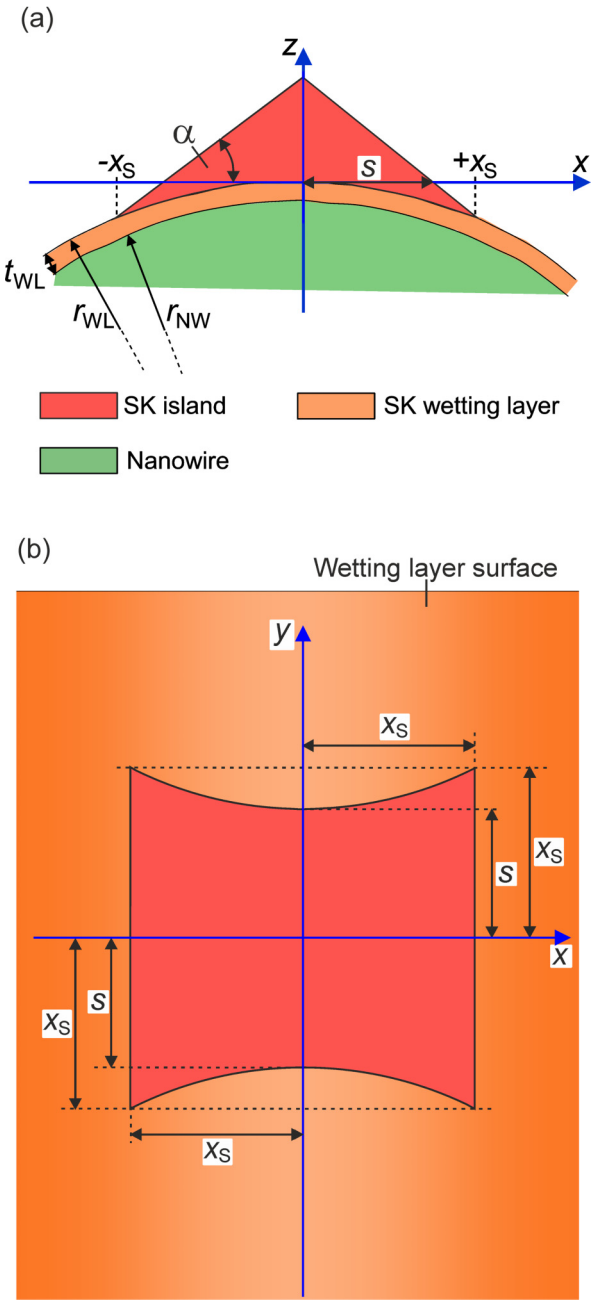

FIG. 1. (a) Cross section and (b) top view drawing illustrating a pyramidal Stranski-Krastanov island on a cylindrical nanowire with the wire axis parallel to y.

respect to planar two-dimensional (2D) growth. Then,

$$\Delta E = \Delta E_{\mathrm{SK}} - \Delta E_{\mathrm{FM}} \tag{1}$$

gives the total-energy difference of the two modes. Here, ΔE, ΔE_{SK}, and ΔE_{FM} refer to Ge deposition onto a region on the NW surface, whose area equals the inverse areal density k of the SK islands. If $\Delta E > 0$, the FM mode is stable, whereas in the case of negative ΔE, SK growth is favored. A detailed calculation of ΔE_{SK} and ΔE_{FM} will be presented later in this section. Overall, ΔE_{SK} and ΔE_{FM} are determined by the surface and elastic relaxation energetics governed by the

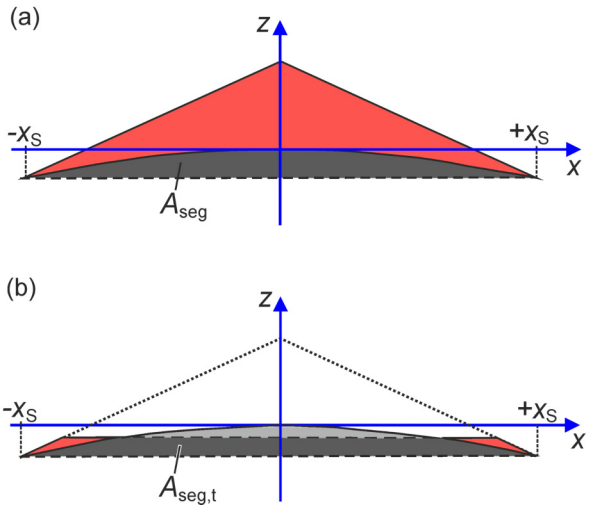

FIG. 2. Schematic cross sections of a pyramidal island on a cylindrical nanowire in the plane perpendicular to the nanowire axis for (a) $y = 0$ and (b) $s < |y| \leqslant x_S$ (cf. Fig. 1). In (b), the silhouette of the pyramid before or behind the section plane is indicated by a dotted line. A_{seg} and $A_{\mathrm{seg,t}}$ are the $x - z$ cross sections of the intersection volume of the pyramid with the wetting layer and nanowire at the respective y positions.

NW substrate geometry in conjunction with the larger lattice constant of the deposited Ge as compared to that of the Si NW.

A. Growth geometry

Let us first focus on the geometrical and structural aspects of our model. We assume that the NW core of radius r_{NW} is covered with a WL of thickness t_{WL} resulting in a total NW radius of $r_{\mathrm{WL}} = r_{\mathrm{NW}} + t_{\mathrm{WL}}$ (Fig. 1). The considered SK island shape is a quadrilateral pyramid with the base edges running parallel and perpendicular to the NW axis, respectively. For convenience, a Cartesian coordinate system is used to describe the geometry, where the y axis runs parallel to the NW axis and the z axis passes through the NW axis and the top of the pyramid. The origin of the coordinate system is placed at the surface of the WL such that the projection of the SK pyramid apex onto the WL is at $x = y = z = 0$. The pyramid facets form an angle α with the $x - y$ plane. The half base length s is measured parallel to the y axis at $x = z = 0$. In the $\pm x$ direction, the pyramid facets intersect the WL surface at $x = \pm x_S$ [Fig. 1(a)] with

$$x_S = \frac{1}{1+\tan^2\alpha}\Big\{\tan\alpha(s\tan\alpha + r_{\mathrm{WL}}) - \Big[\big(r_{\mathrm{WL}}^2 - s^2\big)\tan^2\alpha - 2sr_{\mathrm{WL}}\tan\alpha\Big]^{1/2}\Big\}. \tag{2}$$

The intersection points exist only if $s \leqslant r_{\mathrm{WL}}[(1+\tan^2\alpha)^{1/2} - 1]/\tan\alpha$. A derivation of Eq. (2) and the boundary condition for s is provided in Appendix A. The island volume is calculated as the volume of a pyramid with base length x_S minus its intersection volume with the WL and NW. The intersection volume consists of two parts (Fig. 2): The first is a cylinder segment at $-s \leqslant y \leqslant s$ with $x - z$ cross-section A_{seg}, which is displayed as the dark-gray

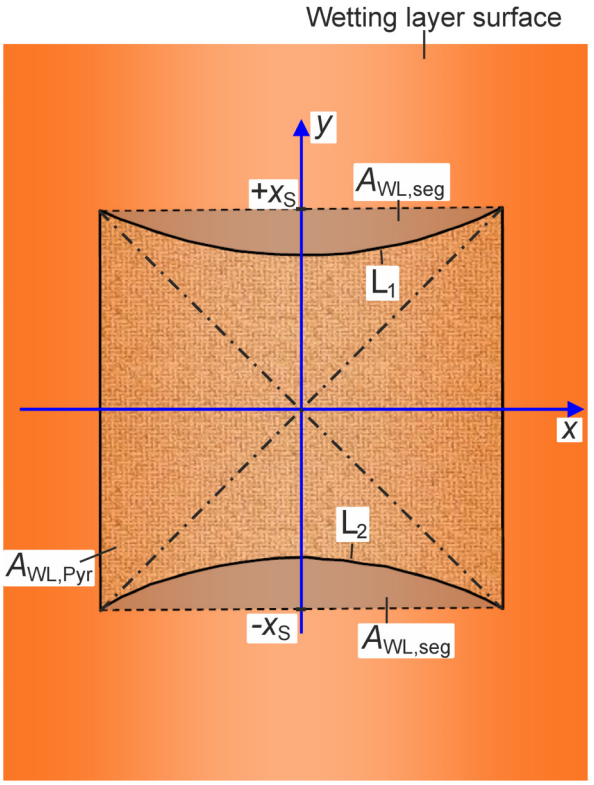

FIG. 3. Top view drawing highlighting the wetting-layer surface area $A_{\mathrm{WL,Pyr}}$ on the cylindrical nanowire (axis parallel to y) beneath the Stranski-Krastanov pyramid island as well as the wetting-layer surface $A_{\mathrm{WL,seg}}$ bound by $y = -x_S$ or $y = +x_S$ and the adjacent pyramid–wetting-layer intersection lines. The top edges of the pyramid are indicated by dash-dotted lines.

area in Fig. 2(a). The second comprises two truncated cylinder segments at $s < y \leqslant x_S$ and $-x_S \leqslant y < -s$ with $x - z$ cross-section $A_{\mathrm{seg,t}}(y)$, shown as the dark-gray area in Fig. 2(b). Thus the volume is

$$V = \frac{4}{3}{x_s}^3 \tan\alpha - \left[2sA_{\mathrm{seg}} + 2\int_s^{x_s} A_{\mathrm{seg,t}}(y)dy\right], \qquad (3)$$

where the integral was solved numerically.

Similarly, the area of the WL surface beneath the pyramid, $A_{\mathrm{WL,Pyr}}$, is given by the WL surface defined by $-x_S \leqslant x \leqslant +x_S$ and $-x_S \leqslant y \leqslant +x_S$ minus twice the WL surface $A_{\mathrm{WL,seg}}$ bound by $y = -x_S$ or $y = +x_S$ and the corresponding pyramid-WL intersection lines L_1 or L_2 (Fig. 3):

$$A_{\mathrm{WL,Pyr}} = 4x_s r_{\mathrm{WL}} \arcsin\left(\frac{x_s}{r_{\mathrm{WL}}}\right) - 2A_{\mathrm{WL,seg}}. \qquad (4)$$

The area $A_{\mathrm{WL,seg}}$ is calculated numerically, as described in Appendix A.

Regarding the strain state of the WL or, more generally, shell layer, a tangential strain ε_t linearly decreasing with radial distance r is assumed. For the Si-nanowire/Ge-shell system, the strain has been analyzed by means of relaxation of the atom positions (i.e., molecular statics) using conjugate gradient energy minimization and the Stillinger-Weber interatomic

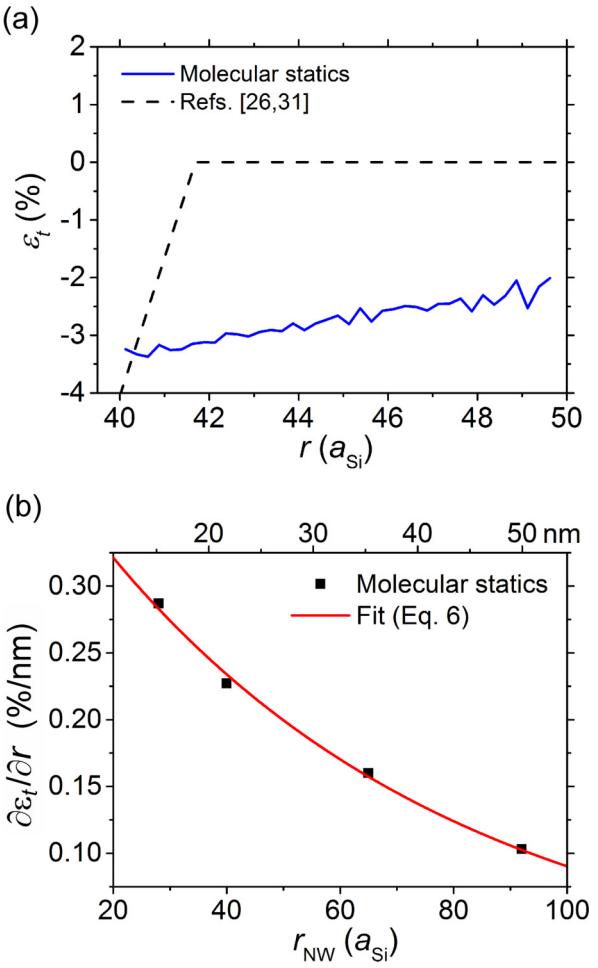

FIG. 4. Results for the strain in a 10-a_{Si}-thick Ge shell on a Si nanowire obtained from molecular statics simulations. (a) Tangential strain ε_t as a function of r for a nanowire radius r_{NW} of $40a_{\mathrm{Si}}$; (b) slope $\partial\varepsilon_t/\partial r$ as a function of nanowire radius.

potential [29] in the LAMMPS software [30]. For the generation of atom coordinates as well as for the strain evaluation, self-written code has been employed. The results show that ε_t is always compressive and decreases approximately linearly with r [Fig. 4(a)]:

$$\varepsilon_t(r) = -\varepsilon_0 + \frac{\partial\varepsilon_t}{\partial r}(r - r_{\mathrm{NW}}) \quad \text{with} \quad r \geqslant r_{\mathrm{NW}}, \qquad (5)$$

where $\varepsilon_0 = (a_{\mathrm{Ge}} - a_{\mathrm{Si}})/a_{\mathrm{Ge}}$ denotes the lattice misfit between the nanowire and its shell. The slope $\partial\varepsilon_t/\partial r$ decays with nanowire radius, which can be described by an exponential fit function [Fig. 4(b)],

$$\frac{\partial\varepsilon_t}{\partial r} = \left(\frac{\partial\varepsilon_t}{\partial r}\right)_0 \exp\left(-\frac{r_{\mathrm{NW}}}{r_c}\right), \qquad (6)$$

where $\partial\varepsilon_t/\partial r$ is in %/nm and r_{NW} is in units of the Si lattice parameter a_{Si}. $(\partial\varepsilon_t/\partial r)_0 \approx 0.441\%/\mathrm{nm}$ and $r_c \approx 63a_{\mathrm{Si}}$ are the fit parameters. In contrast to the model in Refs. [26,31], which assumes a curved lattice of the shell, the slope from molecular statics has a significantly smaller magnitude. In Refs. [26,31], it is supposed that once $\varepsilon_t = 0$ is reached, growth continues strain free, giving rise to the kink of the

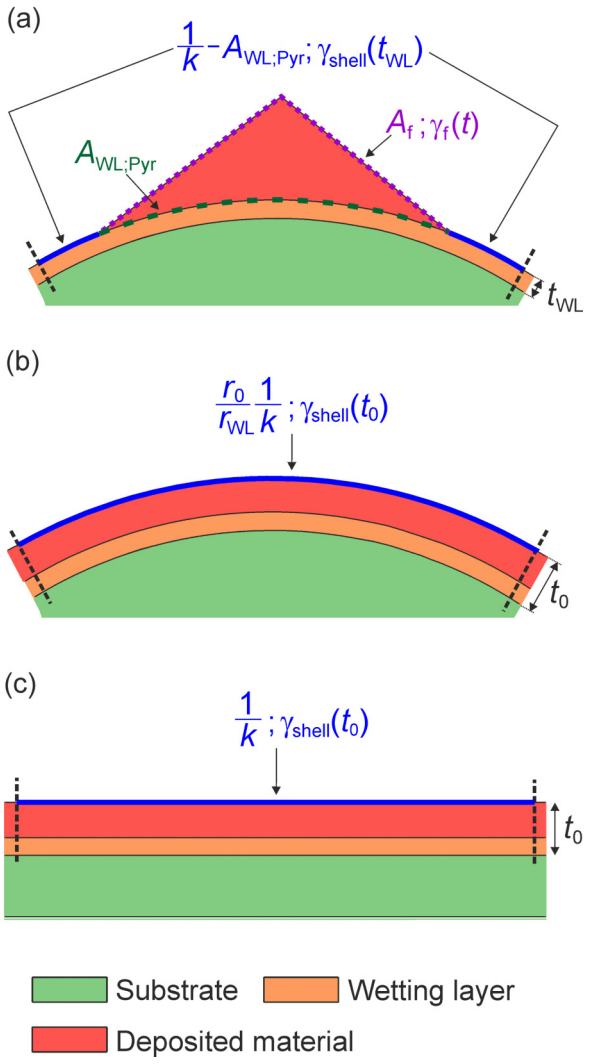

FIG. 5. Schematic cross sections of the growth configurations considered for the growth mode stability analysis: (a) Stranski-Krastanov growth, (b) shell growth, and (c) 2D growth on a planar substrate. In each case, the considered surface areas and surface-energy densities (separated by a semicolon) are given for the region defined by the dashed lines normal to the surface.

dashed line in Fig. 4(a). As the lattice relaxation is not restricted in the radial direction, the normal strain is set to zero, whereas the strain parallel to the NW axis equals $-\varepsilon_0$. Here, the tetragonal lattice distortion due to the Poisson effect is neglected since the shell thickness considered for the analysis of growth-mode stability and thus the corresponding strain relaxation energy are small (Sec. II C).

In the following, we will describe the calculation of the energy differences ΔE_{SK} and ΔE_{FM} upon growth in the SK or FM mode. Figure 5 illustrates the surface areas and energy densities occurring in the two growth modes as opposed to the planar reference system. In all three cases, an area of size $1/k$ on a preexisting WL of thickness t_{WL} is considered. After deposition of a material volume V onto a WL covered planar substrate [Fig. 5(c)], the total layer thickness amounts to $t_0 = t_{WL} + kV$.

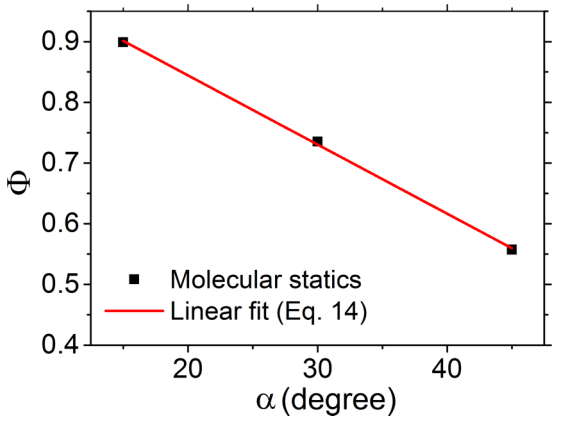

FIG. 6. Correction function Φ in dependence of α for pyramidal Ge islands on a Si nanowire, computed by molecular statics.

B. Energy of Stranski-Krastanov growth

In the case of SK growth [Fig. 5(a)], the energy change with respect to 2D planar growth ΔE_{SK} is determined by the

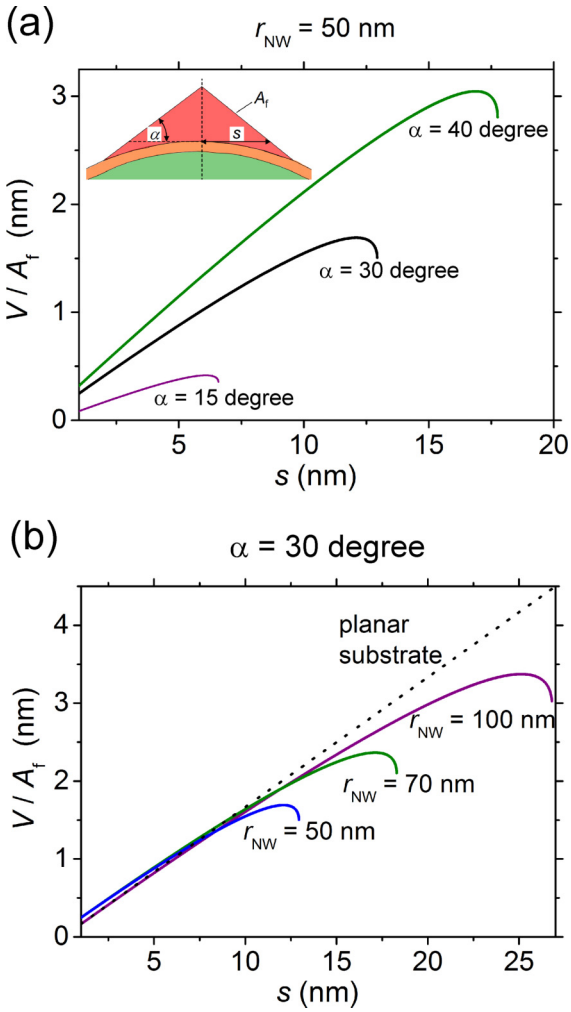

FIG. 7. Pyramid volume-to-surface-area ratio as a function of pyramid half base length s (a) for different pyramid base angles α and $r_{NW} = 50$ nm, and (b) for different nanowire radii r_{NW} and $\alpha = 30°$. The inset in (a) shows a cross-section view of the pyramid on the nanowire along with geometric quantities.

change of surface energy $\Delta E_{\mathrm{SK,surf}}$ due to the enlargement and displacement of the surface and the island elastic relaxation energy $\Delta E_{\mathrm{SK,rel}}$:

$$\begin{aligned}\Delta E_{\mathrm{SK}} &= \Delta E_{\mathrm{SK,surf}} + \Delta E_{\mathrm{SK,rel}} \\ &= \left\{ E_{\mathrm{surf,f}} - E_{\mathrm{surf,WL}} + \frac{1}{k}[\gamma_{\mathrm{shell}}(t_{\mathrm{WL}}) - \gamma_{\mathrm{shell}}(t_0)] \right\} \\ &\quad + \Delta E_{\mathrm{SK,rel}}. \end{aligned} \tag{7}$$

According to Eq. (7), $\Delta E_{\mathrm{SK,surf}}$ is calculated as the total surface energy of the pyramid facets $E_{\mathrm{surf,f}}$ minus the surface energy of the WL beneath the pyramid $E_{\mathrm{surf,WL}}$ plus the surface-energy difference between layers of thicknesses t_{WL} and t_0. $E_{\mathrm{surf,f}}$ is obtained by integration of the surface energy per unit area γ_f over the pyramid facet area A_f:

$$E_{\mathrm{surf,f}} = \int_{A_f} \gamma_f(t)\, dA. \tag{8}$$

As the bonding of the Si substrate lattice affects the first few monolayers of Ge deposited on it via next-neighbor effects, the surface-energy density γ of Ge depends on the distance t to the substrate interface. For a planar substrate/layer configuration, this was quantified by first-principles calculations [32] and approximated by an exponential decay function [28], which we adopt for surface-energy evaluation of the WL and of the pyramid island on the NW:

$$\gamma(t) = \gamma_{\mathrm{NW}} + (\gamma_{\mathrm{Dep},\infty} - \gamma_{\mathrm{NW}})\left[1 - \exp\left(\frac{-t}{h_0}\right)\right]. \tag{9}$$

Here, γ_{NW} and $\gamma_{\mathrm{Dep},\infty}$ denote the surface energies per unit area of the NW substrate and of the infinitely thick deposit strained to match the substrate lattice, and h_0 is the monolayer thickness of the deposit. These surface-energy densities depend on the crystallographic orientation. For the sake of better comparability with previous studies, we use orientationally averaged surface energy densities for Si and Ge. The case of special orientations will be exemplarily considered as well in the last paragraph of Sec. III. The distance of each surface point on the pyramid facets to the WL-NW interface to be inserted in Eq. (8) is computed as $t = t_{\mathrm{WL}} + t_f$, where t_f is the distance of the point to the WL surface. The calculation of t_f is given in Appendix A. $\gamma_{\mathrm{Dep},\infty}$ equals the surface-energy density, which the facets would have at infinite distance to the NW interface, $\gamma_{f,\infty}$, depending on the facet orientation. Similarly, the surface energy of the WL beneath the pyramid island is

$$E_{\mathrm{surf,WL}} = \gamma_{\mathrm{shell}}(t_{\mathrm{WL}}) A_{\mathrm{WL,Pyr}}, \tag{10}$$

where $\gamma_{\mathrm{shell}}(t_{\mathrm{WL}})$ is computed according to Eq. (9) with $\gamma_{\mathrm{Dep},\infty} = \gamma_{\mathrm{shell},\infty}$ (surface-energy density of the cylindrical shell at infinite distance) and $t = t_{\mathrm{WL}}$.

For calculation of the elastic relaxation energy of the pyramidal island, we follow an approach similar to that of Tillmann and Förster [33], which takes the z dependence of the tangential and parallel strain components into account,

$$\Delta E_{\mathrm{SK,rel}} = \frac{Y}{1-\nu}(\Phi^2 - 1)\varepsilon_m^2 V. \tag{11}$$

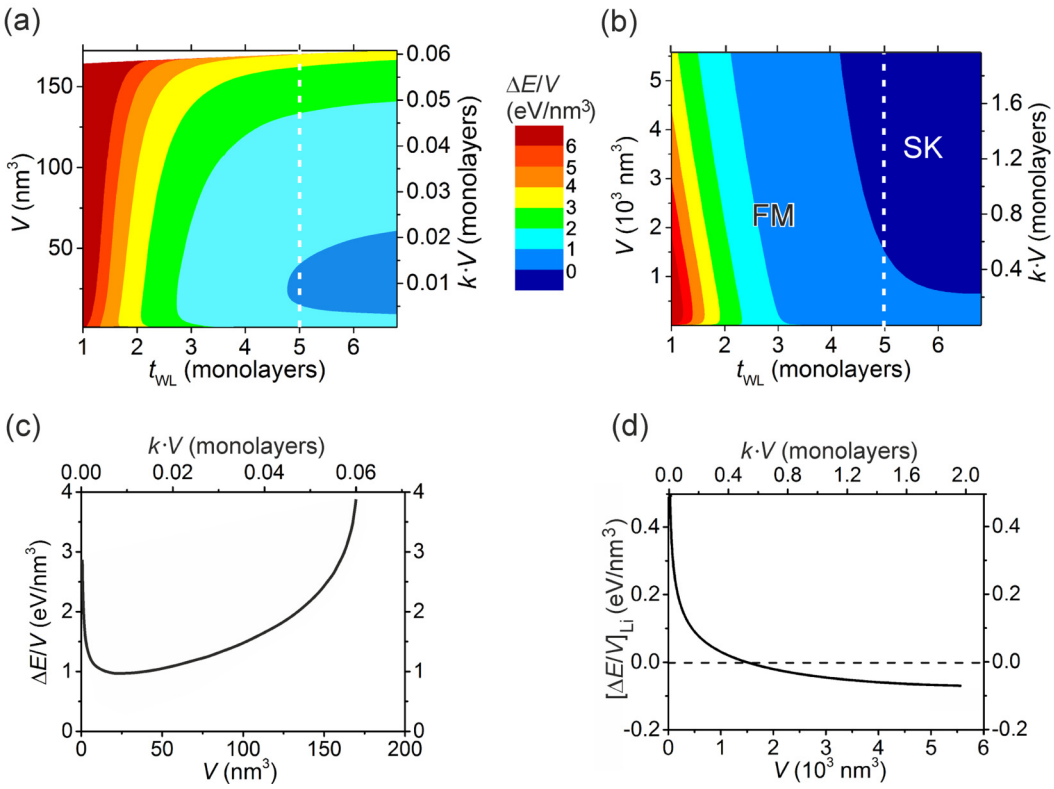

FIG. 8. (a), (b) Contour plots of the total-energy difference ΔE per deposited volume V between Stranski-Krastanov and shell growth as function of wetting-layer thickness and V for a Stranski-Krastanov pyramid base angle of 15° and nanowire radius of 50 nm. (c), (d) Volume profiles of the total-energy difference per volume $\Delta E/V$ for a wetting-layer thickness of five monolayers [marked by dashed lines in (a) and (b)]. Graphs (a) and (c) refer to Eqs. (1)–(16); Graphs (b) and (d) refer to the model of Li and Yang [26].

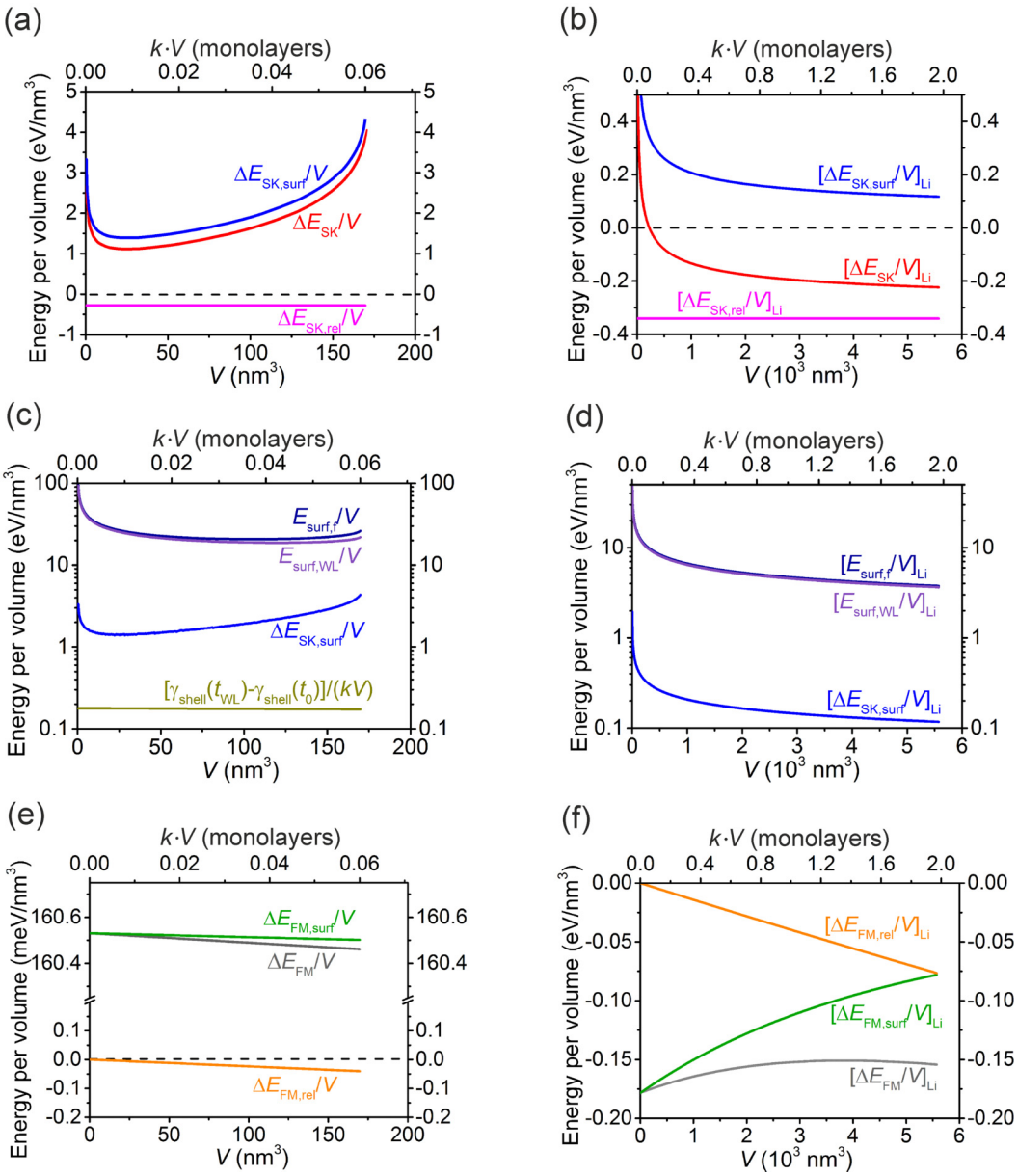

FIG. 9. Volume profiles of the individual energy per volume contributions for a wetting-layer thickness of five monolayers, pyramid base angle of 15°, and nanowire radius of 50 nm: (a)–(d) for the Stranski-Krastanov mode, and (e), (f) for the shell growth mode. Graphs (a), (c), and (e) refer to Eqs. (1)–(16); Graphs (b), (d), and (f) refer to the model of Li and Yang [26].

Y and ν denote the Young's modulus and Poisson ratio of the deposit material, respectively, and ε_m represents the average of the parallel and tangential strain components at the WL surface,

$$\varepsilon_m = \frac{-\varepsilon_0 + \varepsilon_t(r_{\mathrm{WL}})}{2}. \tag{12}$$

Φ describes a dimensionless correction function, which scales with the strain in the island and nanowire substrate, i.e., is inversely related to the strain relaxation,

$$\Phi = \left[\frac{YV\bar{\varepsilon}^2/(1-\nu) + Y_{\mathrm{NW}}V_{\mathrm{NW}}\bar{\varepsilon}_{\mathrm{NW}}^2/(1-\nu_{\mathrm{NW}})}{YV\varepsilon_m^2/(1-\nu)}\right]^{1/2}, \tag{13}$$

where Y_{NW}, ν_{NW} denote the Young's modulus and Poisson ratio of the Si nanowire, and $\bar{\varepsilon}$, $\bar{\varepsilon}_{\mathrm{NW}}$ are the average strains of the Ge island and Si nanowire averaged over the tangential and parallel directions as well as over the strained volumes V and V_{NW}, respectively. Molecular statics simulations are used for determining $\bar{\varepsilon}$ and $\bar{\varepsilon}_{\mathrm{NW}}$. It is found that Φ depends mainly on α and only weakly on island size. The dependence on α can be fitted with a linear equation,

$$\Phi(\alpha) = 1.07 - 0.0114\alpha, \tag{14}$$

where α is in degrees (Fig. 6). The relative error of the island relaxation energy $\Delta E_{\mathrm{SK,rel}}$ due to neglect of the Poisson effect is smaller than 3%.

C. Energy of shell growth

In the case of FM-like shell growth, the material deposition leads to an increase of the cross-section surface area, which is

seen by the material flux. If we assume a constant material flux per unit cross-section area (the same as in the cases of SK growth and 2D planar growth), i.e., a constant deposited volume per unit area and time, a shell of total thickness $t_0 = t_{\mathrm{WL}} + kV$ results, with curvature $r_0 = r_{\mathrm{WL}} + kV$. Like in SK growth, a surface-related term ($\Delta E_{\mathrm{FM,surf}}$) and an elastic-energy term ($\Delta E_{\mathrm{FM,rel}}$) contribute to the total-energy change ΔE_{FM} with respect to 2D planar growth,

$$\Delta E_{\mathrm{FM}} = \Delta E_{\mathrm{FM,surf}} + \Delta E_{\mathrm{FM,rel}}. \tag{15}$$

For the surface contribution, the increase of surface area by the factor r_0/r_{WL} as well as the variation of the surface-energy density γ_{shell} with distance to the NW substrate is taken into account,

$$\Delta E_{\mathrm{FM,surf}} = \frac{1}{k}\gamma_{\mathrm{shell}}(t_0)\left(\frac{r_0}{r_{\mathrm{WL}}} - 1\right) = \gamma_{\mathrm{shell}}(t_0)\frac{V}{r_{\mathrm{WL}}}. \tag{16}$$

The elastic term $\Delta E_{\mathrm{FM,rel}}$ represents the self-relaxation energy, i.e., the gain in elastic energy of the cylindrical heteroepitaxial shell layer as compared to a planar layer, owing to the decay of the tangential strain towards larger radial distance. $\Delta E_{\mathrm{FM,rel}}$ is computed by using linear elasticity theory and Hooke's law; see Appendix B.

For the considered Si-core/Ge-shell structure, the lattice parameter misfit relative to the shell is $\varepsilon_0 \approx 4.03\%$, Young's modulus of Ge and Si are 103 and 130 GPa [34], respectively, the Poisson ratios of Ge and Si are 0.27 and 0.28, respectively [34], and the elastic stiffness coefficients of Ge are $c_{11} = 124$ and $c_{12} = 41.3$GPa (all at room temperature) [35]. Furthermore, a SK island density of $k = 5 \times 10^{13}\mathrm{m}^{-2}$ is assumed, which corresponds to typical experimental values. As reported by Li and Yang [26], the resulting growth-mode stability only weakly depends on the island density. If not, otherwise stated orientation-averaged surface-energy densities of $\gamma_{\mathrm{NW}} = 1.9\,\mathrm{J/m^2}$ for Si and $\gamma_{\mathrm{shell},\infty} = \gamma_{\mathrm{f},\infty} = 1.3\,\mathrm{J/m^2}$ for Ge are used [22,26,36,37].

III. RESULTS AND DISCUSSION

As the SK island volume and surface area play a key role for the growth-mode stability, we first report on the dependence of these geometric quantities on the pyramid half base length s, base angle α, and nanowire radius r_{NW}. Figure 7 displays the evolution of the pyramid volume-to-surface-area ratio as a function of s for different α and r_{NW}. For small s, this ratio agrees well with the corresponding ratio for a pyramid island on a planar substrate, which increases linearly with s. At larger s, the volume-to-surface-area ratio of our model falls increasingly below the linear ratio for the planar substrate, which is explained by the larger peripheral regions of the pyramid characterized by a low thickness. For larger α or r_{NW}, this decrease below the linear ratio is shifted towards larger s. All curves end at large values of s when the pyramid facets no longer intersect the wetting layer.

Figures 8(a) and 8(b) show the total-energy change per deposited volume V as a function of wetting-layer thickness t_{WL} and volume V for a pyramid base angle of 15° and $r_{\mathrm{NW}} = 50$ nm for our model, as opposed to Li and Yang [26]. In this figure and in all following figures (except for Fig. 14 and figures in the Appendices), the thickness of the deposited material kV, corresponding to the volume V, is also displayed

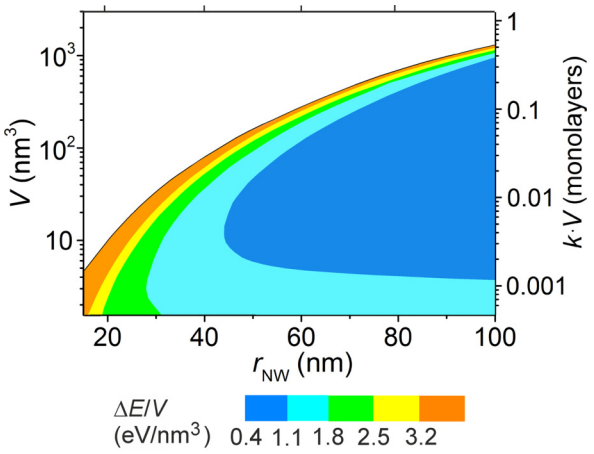

FIG. 10. Total-energy difference ΔE per deposited volume V between Stranski-Krastanov and shell growth as a function of nanowire radius and V for a Stranski-Krastanov pyramid base angle of 15° and wetting-layer thickness of five monolayers, according to the model presented here.

in units of monolayers on the right or top axis. Within the analyzed ranges of t_{WL} and V for our model, the FM-like shell growth mode is stable ($\Delta E > 0$), whereas Li and Yang predict the SK mode to become stable at larger t_{WL} and V [dark-blue region in Fig. 8(b)]. In contrast to Li and Yang, our results show that for $t_{\mathrm{WL}} \geqslant 2.5$ monolayers, $\Delta E/V$ passes through a minimum at intermediate V and rises at larger V [Figs. 8(a) and 8(c) versus 8(b) and 8(d)]. In the following, we exemplarily analyze this behavior with the help of the volume profiles of the individual SK and FM energy contributions for a WL thickness of 5 monolayers, which is close to the experimentally observed WL thickness (Fig. 9) [12]. The initial decrease of $\Delta E/V$ with increasing volume [Figs. 9(a) and 9(c)] originates from a decrease of $\Delta E_{\mathrm{SK,surf}}/V$ mainly owing to an increase of the volume-to-facet surface-area ratio, which leads to a decrease of the difference between the facet surface energy and the surface energy of the WL beneath the island per volume, respectively [Fig. 9(c)]. In the model of Li and Yang, this effect dominates the dependence of $\Delta E/V$ on V in the entire volume range [Figs. 9(b) and 9(d)]. Please note that the model of Li and Yang uses a reference state with a surface-energy density of $\gamma_{\mathrm{shell}}(t_{\mathrm{WL}})$, i.e., $[\Delta E_{\mathrm{SK,surf}}/V]_{\mathrm{Li}} = [E_{\mathrm{surf,f}}/V]_{\mathrm{Li}} - [E_{\mathrm{surf,WL}}/V]_{\mathrm{Li}}$ [26]. In our model, for large island volumes, the volume-to-facet surface-area ratio declines and, moreover, the facet-area portion having a small distance to the WL increases due to the NW curvature, leading to an increased surface-energy density. These effects result in an increase of $E_{\mathrm{surf,f}}/V$ relative to $E_{\mathrm{surf,WL}}/V$ and thus in an increase of $\Delta E_{\mathrm{SK,surf}}/V$ [Fig. 9(c)]. In contrast, this increase of $\Delta E_{\mathrm{SK,surf}}/V$ does not occur in the model of Li and Yang, which assumes a volume-to-facet surface-area ratio increasing linearly with V, as is the case on a planar substrate, and a constant island facet surface-energy density. As compared to the SK energy changes, the corresponding surface- and elastic-energy changes per volume in the case of FM growth [Fig. 9(e)] are one-to-two or three-to-four orders of magnitude smaller, respectively. On the one hand, the surface energy per volume, $\Delta E_{\mathrm{FM,surf}}/V$, slightly decreases because of the rela-

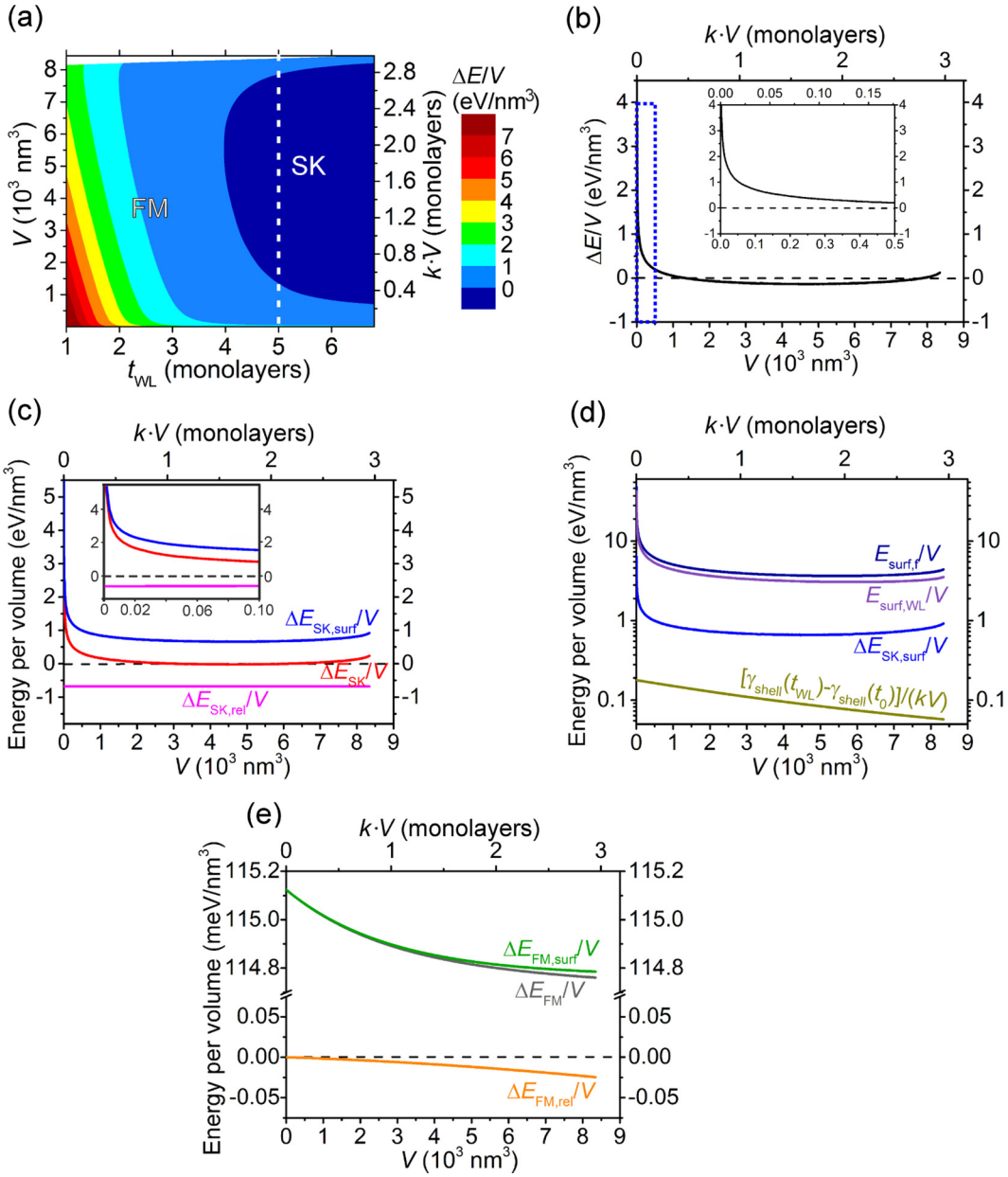

FIG. 11. (a) Total-energy difference ΔE per deposited volume V between Stranski-Krastanov and shell growth as a function of wetting-layer thickness and V for a Stranski-Krastanov pyramid base angle of 30° and nanowire radius of 70 nm. (b)–(e) Volume profiles of the individual energy per volume contributions for a wetting-layer thickness of five monolayers [marked by a vertical dashed line in (a)]: (b) total energy $\Delta E/V$; (c), (d) Stranski-Krastanov mode; and (e) shell growth mode. The insets in (b) and (c) are enlargements of regions at low volume, respectively.

tively small decrease of $\gamma_{\text{shell}}(t_0)$ with increasing t_0 or V. On the other hand, $\Delta E_{\text{FM,rel}}/V$ becomes increasingly negative, as a larger portion of the shell lattice is at a larger distance to the NW core and therefore more relaxed. In contrast, $\Delta E_{\text{FM,surf}}/V$ and therefore $\Delta E_{\text{FM}}/V$ are negative in the approach of Li and Yang [Fig. 9(f)] because it uses $\gamma(t_{\text{WL}})$ instead of $\gamma(t_0)$ as the energy density of the reference surface.

If we now look at the dependence of $\Delta E/V$ on the NW radius r_{NW} (Fig. 10), we find that $\Delta E/V$ decreases with increasing r_{NW} (indicating a decreasing stability of the shell growth mode), but remains positive for $r_{\text{NW}} \leqslant 100$ nm. As our approach neglects the dependence of nanowire surface energy on curvature, only nanowire radii $r_{\text{NW}} \geqslant 15$ nm are considered.

At a larger pyramid base angle of 30° and $r_{\text{NW}} = 50$ nm, the FM mode is still stable for all volumes and WL thicknesses below seven monolayers (not shown). For a larger NW radius $r_{\text{NW}} = 70$ nm and an angle of 30°, the SK mode occurs in a wide volume interval for WL thicknesses above four monolayers [Fig. 11(a)]. The transition from the FM to the SK mode is governed by the surface-energy change per volume in the SK mode, $\Delta E_{\text{SK,surf}}/V$ [Figs. 11(b) and 11(c)], similarly to the case of Fig. 9 ($r_{\text{NW}} = 50$ nm, $\alpha = 15°$). For small volumes, $\Delta E_{\text{SK,surf}}/V$ decreases with V, like in the case $r_{\text{NW}} = 50$ nm, $\alpha = 15°$, which gives rise to a first zero crossing $\Delta E/V$ at $V \approx 1.3 \times 10^3$ nm^3 (0.46 monolayers) for $t_{\text{WL}} = 5$ monolayers. For large volumes, the volume-to-facet surface-

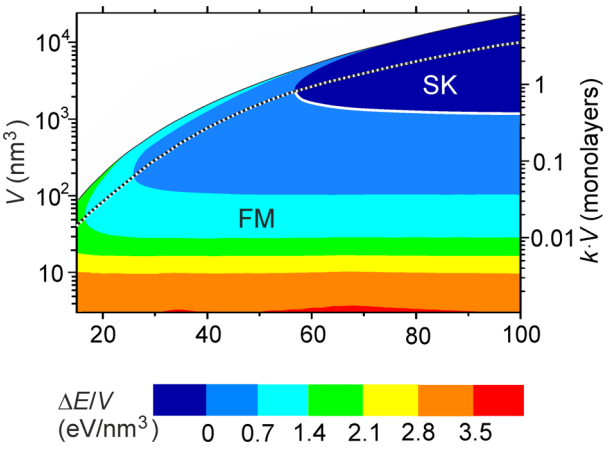

FIG. 12. Total-energy difference ΔE per deposited volume V between Stranski-Krastanov and shell growth as a function of nanowire radius and V for a Stranski-Krastanov pyramid base angle of 30° and wetting-layer thickness of five monolayers. The black/white dotted line indicates the minimum which occurs in the $\Delta E/V$ volume profiles. The white solid line highlights the critical volume for the transition from shell to Stranski-Krastanov mode as a function of nanowire radius.

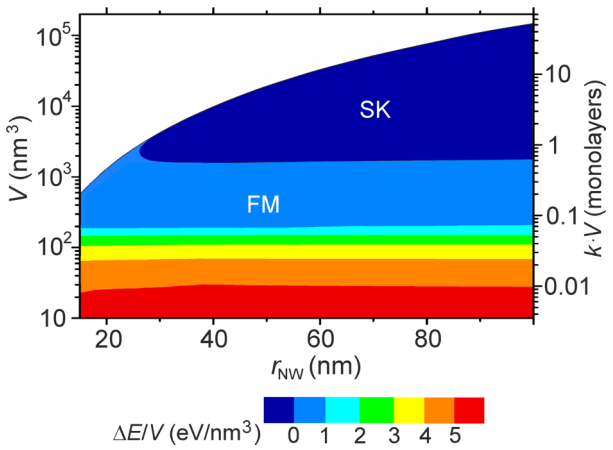

FIG. 13. Total-energy difference ΔE per deposited volume V between Stranski-Krastanov and shell growth as a function of nanowire radius and V for a Stranski-Krastanov pyramid base angle of 45° and a wetting-layer thickness of five monolayers.

area ratio declines, leading to an increase of $\Delta E_{\mathrm{SK,surf}}/V$ and, consequently, to a second zero crossing of $\Delta E_{\mathrm{SK}}/V$ and $\Delta E/V$ at $V \approx 7.9 \times 10^3\,\mathrm{nm}^3$ (2.8 monolayers). Compared to $r_{\mathrm{NW}} = 50\,\mathrm{nm}$, $\alpha = 15°$, the contribution of the peripheral pyramid facet regions (with a low distance between the surface and the WL) to the pyramid surface energy is less pronounced for $r_{\mathrm{NW}} = 70\,\mathrm{nm}$, $\alpha = 30°$; therefore, the increase of $\Delta E_{\mathrm{SK,surf}}/V$ at large volumes [Fig. 11(d)] is less pronounced in the latter case. In addition, the magnitude of $\Delta E_{\mathrm{SK,rel}}/V$ exceeds that for $r_{\mathrm{NW}} = 50\,\mathrm{nm}$, $\alpha = 15°$ [Fig. 11(c) versus Fig. 9(a)], owing to the stronger relaxation in the upper parts of the island for $\alpha = 30°$. Again, the surface- and elastic-energy changes per volume in the case of FM growth remain comparatively small, with decreasing $\Delta E_{\mathrm{FM,surf}}/V$ and increasingly negative $\Delta E_{\mathrm{FM,rel}}/V$ towards larger V [Fig. 11(e)]. Figure 12 exhibits $\Delta E/V$ in dependence of r_{NW} and V for $\alpha = 30°$ and $t_{\mathrm{WL}} = 5$ monolayers. The calculations show that for $r_{\mathrm{NW}} \geqslant 57\,\mathrm{nm}$, a SK stability region evolves for a wide volume range above a critical volume ranging between 1800 and 1180 nm^3 (0.64 to 0.42 monolayers). As expected, this critical volume V_{crit} decreases towards larger NW radius because the larger pyramid volume-to-facet surface-area ratio leads to a stronger decrease of $\Delta E_{\mathrm{SK,surf}}/V$ with V. As already discussed for $r_{\mathrm{NW}} = 50\,\mathrm{nm}$, $\alpha = 15°$ and $r_{\mathrm{NW}} = 70\,\mathrm{nm}$, $\alpha = 30°$, a minimum of $\Delta E/V$ occurs in the volume profiles for each r_{NW}, marked by the dotted line in Fig. 12. Consequently, a second SK-FM transition appears for NW radii between 57 and 74 nm. For $r_{\mathrm{NW}} > 74\,\mathrm{nm}$, this transition does not exist because the SK mode remains stable up to the largest possible SK island size.

When increasing the pyramid base angle to 45°, a larger SK stability zone is observed, which is shifted to larger volumes and which extends to smaller NW radii (down to 27 nm) for a WL thickness of five monolayers (Fig. 13). The enlarged SK zone can be explained by the larger SK volume-to-facet surface-area ratio in combination with the stronger elastic relaxation of the SK island, i.e., more negative $\Delta E_{\mathrm{SK,rel}}/V$. These factors also explain the decrease of the critical NW radius $r_{\mathrm{NW,crit}}$, i.e., the minimum NW radius for which SK growth is stable, with increasing pyramid base angles α (Fig. 14).

Lastly, let us consider the special case of a SK island bounded by (112), $(\bar{1}\bar{1}2)$, $(\bar{1}12)$, and $(1\bar{1}2)$ facets with $\alpha \approx 35.3°$ against the (001) island basal plane. We have selected this case because {112} facets have a low surface-energy density and exhibit an angle α in the range between 20° and 45° as observed in experiments [12]. For the Ge shell, we use $\gamma_{\mathrm{shell},\infty} = 1.3\,\mathrm{J/m}^2$ as before, and for the {112} island facets, we use $\gamma_{\mathrm{f},\infty} = 1.1\,\mathrm{J/m}^2$, obtained by extrapolation from silicon data [37]. As apparent from Fig. 15, the reduced surface energy of the island facets leads to a stabilization of the SK mode throughout the entire analyzed ranges of deposited volumes and NW radii. The finding that the SK mode becomes stable only in the presence of larger pyramid base angles or low-energy island facets agrees with experimental

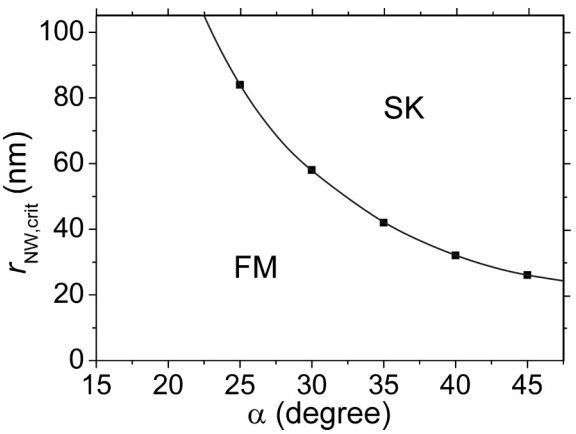

FIG. 14. Critical nanowire radius $r_{\mathrm{NW,crit}}$, i.e., the minimum NW radius for which Stranski-Krastanov growth is stable, as a function of pyramid base angle α at a wetting-layer thickness of five monolayers. The solid line serves as a guide to the eye.

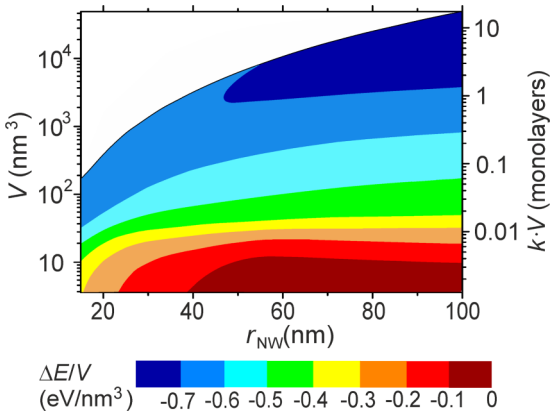

FIG. 15. Total-energy difference ΔE per deposited volume V between Stranski-Krastanov and shell growth as a function of the nanowire radius and V for a preexisting wetting-layer thickness of five monolayers, a pyramid base angle of 35.3° [corresponding to {112} pyramid facets and a (001) island basal plane], and $\gamma_{f,\infty} = 1.1\,\mathrm{J/m^2}$, $\gamma_{shell,\infty} = 1.3\,\mathrm{J/m^2}$.

observations [12]. In particular, the presence of low-energy island facets would explain the reported growth of Ge islands on Si NWs of small diameter (≈ 20 nm) [24].

IV. CONCLUSIONS

In summary, we have analyzed the thermodynamic stability of the coherent heteroepitaxial shell and Stranski-Krastanov growth modes on cylindrical nanowire substrates by using an improved model. Contrary to previous theoretical studies, we consider the exact geometrical shape of the pyramidal islands on the nanowire, the dependence of the island relaxation energy on the pyramid base angle, and the dependence of the island surface-energy density on the distance to the nanowire substrate. Applied to the growth of Ge on cylindrical Si NWs, our approach predicts that the FM-like shell growth mode occurs for low pyramid base angles (15°), whereas at larger angles, the SK mode is favored above a critical NW radius. Low-energy island surface facets, which form larger angles (>30°) against the island basal plane, are found to stabilize the SK mode strongly for all NW radii in a wide range of deposited volumes. This result agrees with experiments.

ACKNOWLEDGMENT

The authors are grateful to Deutsche Forschungsgemeinschaft for financial support under Grants No. RI 2655/1-1 and No. LI 449/16-1.

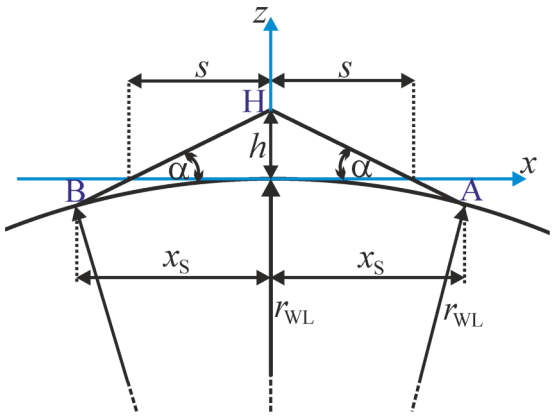

FIG. 16. Cross section of a quadrilateral pyramid island on the radial surface of a cylinder. The lengths and points used for calculation of the distance x_S are sketched.

APPENDIX A: GEOMETRIC PROPERTIES OF A PYRAMIDAL ISLAND ON THE RADIAL SURFACE OF A CYLINDER

1. Intersections between the $\pm x$ pyramid facets and the cylinder surface

Figure 16 depicts the $x - z$ cross section of a quadrilateral pyramid island with half base length s and angle α situated on the radial surface of a cylinder (axis parallel to y). The origin of the coordinate system, i.e., $z = 0$, is at the cylinder surface. The x positions of the intersections between the $\pm x$ pyramid facets and the cylinder surface, $\pm x_S$, are calculated as follows. On the one hand, the line HA on the pyramid facet is given by

$$z_L(x) = h - x\tan\alpha = (s - x)\tan\alpha, \tag{A1}$$

where h is the pyramid height. On the other hand, the circle representing the cylinder circumference can be expressed by

$$z_{Circle}(x) = \left(r_{WL}^2 - x^2\right)^{1/2} - r_{WL}, \tag{A2}$$

where r_{WL} represents the radius of the nanowire including the wetting layer. At the intersection point A, $z_L(x_S) = z_{Circle}(x_S)$, which yields the quadratic equation

$$(1 + \tan^2\alpha)x_S^2 - 2\tan\alpha(s\tan\alpha + r_{WL})x_S + s\tan\alpha(s\tan\alpha + 2r_{WL}) = 0. \tag{A3}$$

Solving Eq. (A3) gives the x coordinate of point A:

$$x(A) = x_s = \frac{\tan\alpha(s\tan\alpha + r_{WL}) - \left[\left(r_{WL}^2 - s^2\right)\tan^2\alpha - 2sr_{WL}\tan\alpha\right]^{1/2}}{1 + \tan^2\alpha}. \tag{A4a}$$

Owing to the mirror symmetry, we obtain, for the x coordinate of point B,

$$x(B) = -x_s = -\frac{\tan\alpha(s\tan\alpha + r_{WL}) - \left[\left(r_{WL}^2 - s^2\right)\tan^2\alpha - 2sr_{WL}\tan\alpha\right]^{1/2}}{1 + \tan^2\alpha}. \tag{A4b}$$

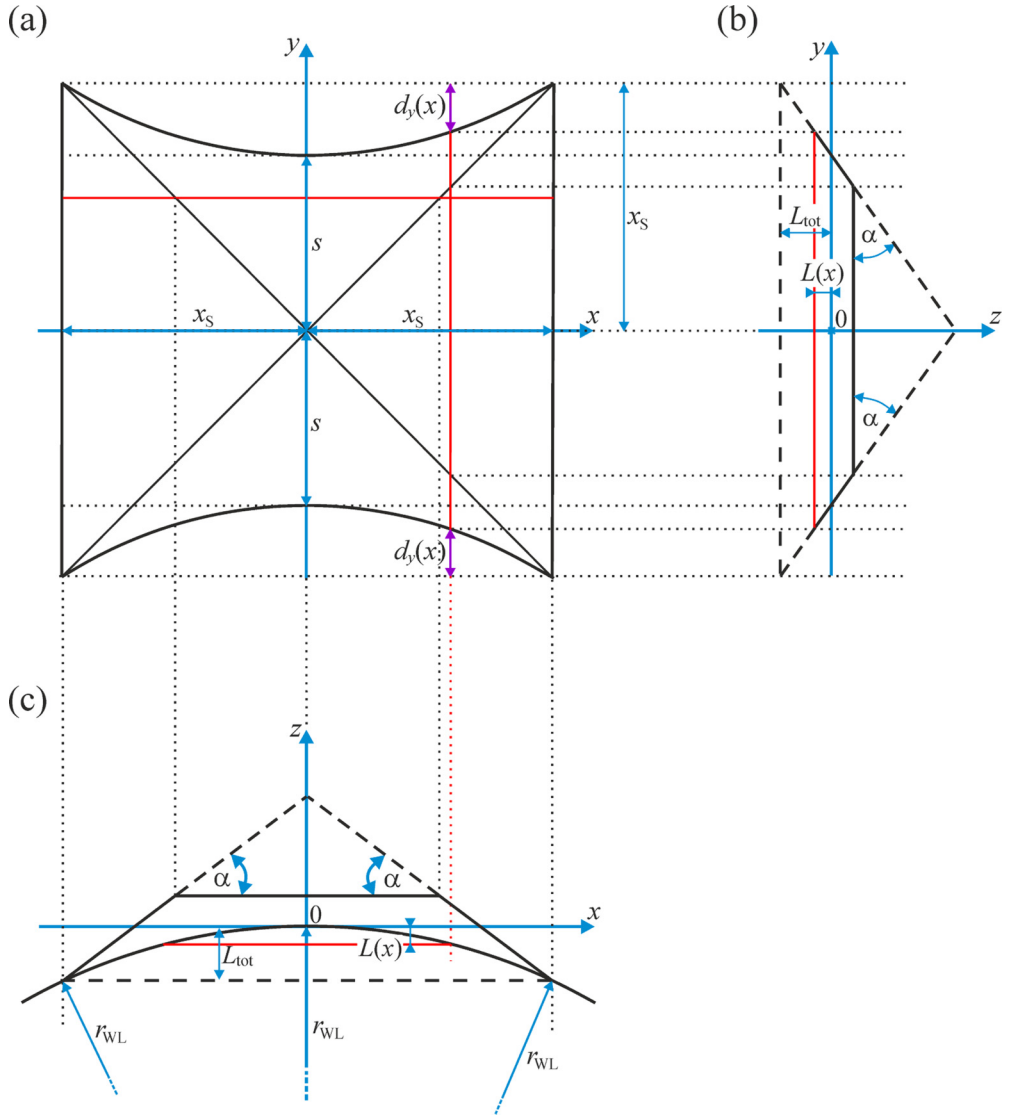

FIG. 17. (a) Top view of a Stranski-Krastanov island of quadrilateral pyramid shape, which is situated on the nanowire radial surface covered by a wetting layer. (b), (c) Sections in the $y-z$ and $x-z$ planes along the two red lines in (a). The distances used for the calculation of $d_y(x)$ [Eq. (A8)] are displayed.

The intersection points A and B exist only if Eq. (A3) has real-valued solutions, i.e., if the argument of the square root in Eqs. (A4a) and (A4b) is zero or positive:

$$\left(r_{\mathrm{WL}}^2 - s^2\right)\tan^2\alpha - 2sr_{\mathrm{WL}}\tan\alpha \geqslant 0$$

$$\Leftrightarrow s \leqslant s_{\mathrm{crit}} = r_{\mathrm{WL}}[(1+\tan^2\alpha)^{1/2} - 1]/\tan\alpha. \quad \text{(A5)}$$

This means that the pyramid half base length s is always below or equal to the critical half base length s_{crit}. For example, $s_{\mathrm{crit}} = 13.4\,\mathrm{nm}$ for $r_{\mathrm{WL}} = 50\,\mathrm{nm}$ and $\alpha = 30^\circ$.

2. Wetting-layer surface $A_{\mathrm{WL,seg}}$

Next, we consider the wetting-layer (WL) surface $A_{\mathrm{WL,seg}}$ bound by $y = +x_S$ or $y = -x_S$ and the corresponding pyramid-WL intersection lines L_1 or L_2 (Fig. 3). $A_{\mathrm{WL,seg}}$ is required for the calculation of the area of the WL surface covered by the pyramid. $A_{\mathrm{WL,seg}}$ is obtained by numerical integration along x of the distance d_y between $y = +x_S$ or $y = -x_S$ and L_1 or L_2,

$$A_{\mathrm{WL,seg}} = \int_{-x_S}^{x_S} d_y(x)dx. \quad \text{(A6)}$$

According to Fig. 17, the distance $d_y(x)$ is a function of the x position and given by

$$d_y(x) = \frac{L_{\mathrm{tot}} - L(x)}{\tan\alpha}. \quad \text{(A7)}$$

With $L_{\mathrm{tot}} = \tan\alpha(x_S - s)$ and $L(x) = r_{\mathrm{WL}} - (r_{\mathrm{WL}}^2 - x^2)^{1/2}$, we obtain

$$d_y(x) = x_S - s - \frac{r_{\mathrm{WL}} - \left(r_{\mathrm{WL}}^2 - x^2\right)^{1/2}}{\tan\alpha}. \quad \text{(A8)}$$

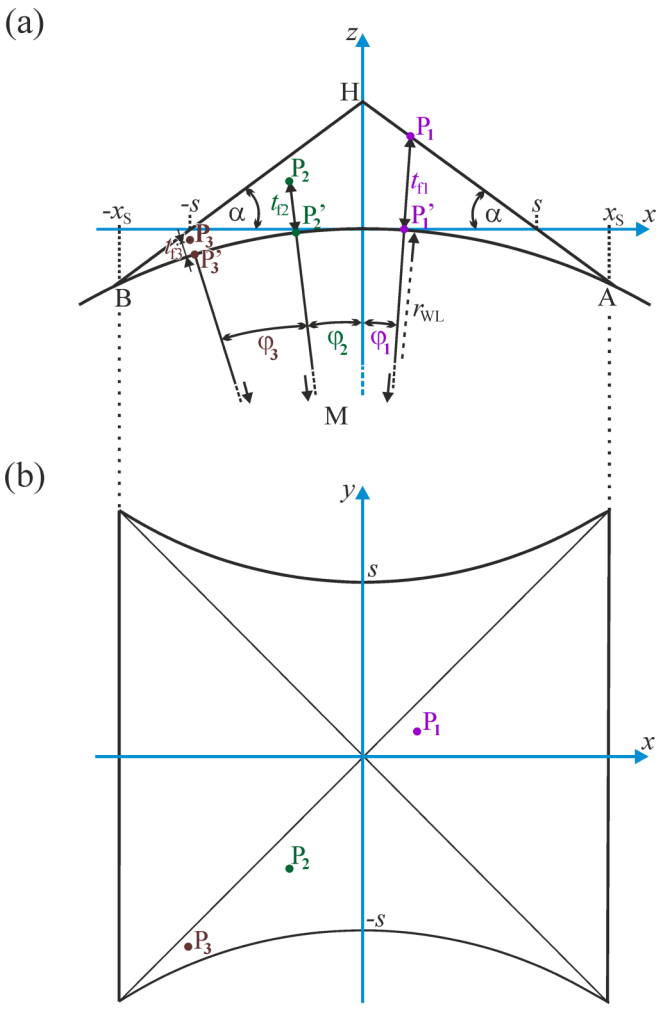

FIG. 18. (a) Cross-section view and (b) top view of a Stranski-Krastanov island of quadrilateral pyramid shape, which is situated on the nanowire radial surface covered by a wetting layer. Different surface points P_1, P_2, P_3 on the island are marked as well as the geometric quantities used for the calculation of the distance t_f between theses points and the wetting-layer surface. In (a), P_1, P_1', P_2, P_2', P_3, and P_3' are projected onto the $x-z$ section plane at $y=0$.

3. Distance of pyramid surface points to the underlying nanowire wetting layer

Figure 18 illustrates the distance t_f of surface points on a pyramidal island to the nanowire wetting layer. If $P(x_P; y_P; z_P)$ denotes a surface point and $P'(x_{P'}; y_{P'}; z_{P'})$ ($y_{P'} = y_P$) denotes the corresponding point defined by the intersection between the radial line MP (M: point on the wire axis with $y_M = y_P$) and the wetting-layer surface, this distance is

$$t_f = \overline{PP'} = [(x_P - x_{P'})^2 + (z_P - z_{P'})^2]^{1/2}. \tag{A9}$$

For given $x_{P'}$, the angle φ between the line MP and the z axis is

$$\varphi = \arcsin\left(\frac{x_{P'}}{r_{WL}}\right). \tag{A10}$$

For convenience, we define that $\varphi > 0$ if $x > 0$ and $\varphi < 0$ if $x < 0$. Therefore, the equation for the line MP is

$$z(x) = -r_{WL} + x \cdot \tan\left(\frac{\pi}{2} - \varphi\right), \tag{A11}$$

which allows one to calculate $z_{P'}$, the z coordinate of P', by substituting x by $x_{P'}$. The coordinates of P are obtained as follows. In the case of the $\pm x$ pyramid facets (points P_1, P_1' in Fig. 18; $|y_{P'}| \leqslant |x_{P'}|$), the intersection of the line MP with the line HA yields

$$x_P = \frac{r_{WL} + s\tan\alpha}{\tan\alpha + \tan(\pi/2 - \varphi)}. \tag{A12}$$

z_P is obtained by substituting x by x_P in Eq. (A11).

In the case of the $\pm y$ pyramid facets (points P_2, P_2' and P_3, P_3' in Fig. 18, $|x_{P'}| \leqslant |y_{P'}|$) we calculate x_P as the x coordinate of the intersection of the line MP with the line $z = z_P = \tan\alpha(s - |y_P|)$,

$$x_P = \frac{r_{WL} + \tan\alpha(s - |y_P|)}{\tan(\pi/2 - \varphi)}. \tag{A13}$$

For those points on the $\pm y$ facets for which $|y_P| > s$ (e.g., point P_3), the additional restriction $|x_P| \geqslant x_C$ holds. x_C denotes the x coordinate magnitude of the intersection points of a $x-z$ wire section with the curved pyramid wetting-layer intersection lines L_1 or L_2,

$$x_C = \{(y - s)[2r_{WL} - (y - s)\tan\alpha]\tan\alpha\}^{1/2}. \tag{A14}$$

APPENDIX B: SELF-RELAXATION ENERGY OF A HETEROEPITAXIAL CYLINDRICAL SHELL

The self-relaxation energy of the heteroepitaxial cylindrical shell on the nanowire is quantified on the basis of linear elasticity theory and Hooke's law. According to the assumed strain state in the cylindrical shell solely, the strain components in the directions parallel and tangential to the nanowire are nonzero and the tangential component $\varepsilon_t(r)$ depends on the radial distance r. For the calculation of the strain energy density of the heteroepitaxial cylindrical shell on the nanowire, we write the strain and stress tensors in Voigt notation:

$$\varepsilon = \begin{pmatrix}\varepsilon_0\\ \varepsilon_t\\ 0\\ 0\\ 0\\ 0\end{pmatrix}, \sigma = C\varepsilon = \begin{pmatrix} c_{11} & c_{12} & c_{12} & 0 & 0 & 0\\ c_{12} & c_{11} & c_{12} & 0 & 0 & 0\\ c_{12} & c_{12} & c_{11} & 0 & 0 & 0\\ 0 & 0 & 0 & c_{44} & 0 & 0\\ 0 & 0 & 0 & 0 & c_{44} & 0\\ 0 & 0 & 0 & 0 & 0 & c_{44}\end{pmatrix}\begin{pmatrix}\varepsilon_0\\ \varepsilon_t\\ 0\\ 0\\ 0\\ 0\end{pmatrix} = \begin{pmatrix} c_{11}\varepsilon_0 + c_{12}\varepsilon_t\\ c_{12}\varepsilon_0 + c_{11}\varepsilon_t\\ 0\\ 0\\ 0\\ 0\end{pmatrix}, \tag{B1}$$

where C denotes the elastic stiffness matrix in the case of cubic crystal symmetry. Then the strain energy density (energy per unit volume) $w(r)$ is given by

$$w(r) = \tfrac{1}{2}\sigma\varepsilon = \tfrac{1}{2}c_{11}\left(\varepsilon_0^2 + \varepsilon_t^2\right) + c_{12}\varepsilon_0\varepsilon_t. \tag{B2}$$

Multiplication of Eq. (B2) with the nanowire circumference and integration over r yields the elastic strain energy $\Delta E_{\mathrm{FM,el}}$ per nanowire length L of the shell for the entire circumference,

$$\frac{\Delta E_{\mathrm{FM,el}}}{L} = \int_{r_{\mathrm{WL}}}^{r_0} 2\pi r w(r) dr. \tag{B3}$$

For a shell (radius r_0) deposited onto a preexisting wetting layer (radius r_{WL}), the integration runs from $r = r_{\mathrm{WL}}$ to $r = r_0$ with $\varepsilon_t(r)$ given by Eq. (5).

As we consider an area of the size k^{-1} (k: Stranski-Krastanov island areal density), which has a quadratic shape with length $k^{-1/2}$, Eq. (B3) is multiplied with the length $k^{-1/2}$ and with the fraction $k^{-1/2}/(2\pi r_{\mathrm{WL}})$ relating the square edge length to the total nanowire circumference. By subtraction of the strain energy in the case of planar growth of the same amount of material, $V w(r_{\mathrm{WL}})$, we obtain the self-relaxation energy $\Delta E_{\mathrm{FM,rel}}$ of the deposited shell:

$$\begin{aligned}\Delta E_{\mathrm{FM,rel}} = \frac{1}{2kr_{\mathrm{WL}}}\Bigg\{&\left[\left(\varepsilon_0^2 - \varepsilon_0\frac{\partial\varepsilon_t}{\partial r}r_{\mathrm{NW}}\right)(c_{11}+c_{12}) + \frac{c_{11}}{2}r_{\mathrm{NW}}^2\left(\frac{\partial\varepsilon_t}{\partial r}\right)^2\right]\left(r_0^2 - r_{\mathrm{WL}}^2\right)\\ &+\frac{2}{3}\frac{\partial\varepsilon_t}{\partial r}\left[\varepsilon_0(c_{11}+c_{12}) - c_{11}\frac{\partial\varepsilon_t}{\partial r}r_{\mathrm{NW}}\right]\left(r_0^3 - r_{\mathrm{WL}}^3\right) + \frac{c_{11}}{4}\left(\frac{\partial\varepsilon_t}{\partial r}\right)^2\left(r_0^4 - r_{\mathrm{WL}}^4\right)\Bigg\}\\ &- V\Bigg\{c_{11}\left[\varepsilon_0^2 + \varepsilon_0\frac{\partial\varepsilon_t}{\partial r}(r_{\mathrm{WL}} - r_{\mathrm{NW}}) + \frac{1}{2}\left(\frac{\partial\varepsilon_t}{\partial r}\right)^2(r_{\mathrm{WL}} - r_{\mathrm{NW}})^2\right] + c_{12}\varepsilon_0\left[\varepsilon_0 + \frac{\partial\varepsilon_t}{\partial r}(r_{\mathrm{WL}} - r_{\mathrm{NW}})\right]\Bigg\}.\end{aligned} \tag{B4}$$

[1] M. T. Björk, B. J. Ohlsson, T. Sass, A. I. Persson, C. Thelander, M. H. Magnusson, K. Deppert, L. R. Wallenberg, and L. Samuelson, One-dimensional steeplechase for electrons realized, Nano Lett. **2**, 87 (2002).

[2] L. J. Lauhon, M. S. Gudiksen, D. Wang, and C. M. Lieber, Epitaxial core-shell and core-multishell nanowire heterostructures, Nature (London) **420**, 57 (2002).

[3] K. L. Kavanagh, I. Saveliev, M. Blumin, G. Swadener, and H. E. Ruda, Faster radial strain relaxation in InAs-GaAs core-shell heterowires, J. Appl. Phys. **111**, 044301 (2012).

[4] Y. Jung, D.-K. Ko, and R. Agarwal, Synthesis and structural characterization of single-crystalline branched nanowire heterostructures, Nano Lett. **7**, 264 (2007).

[5] M. Paladugu, J. Zou, G. J. Auchterlonie, Y. N. Guo, Y. Kim, H. J. Joyce, Q. Gao, H. H. Tan, and C. Jagadish, Evolution of InAs branches in InAs/GaAs nanowire heterostructures, Appl. Phys. Lett. **91**, 133115 (2007).

[6] Q. Gao, H. H. Tan, H. E. Jackson, L. M. Smith, J. M. Yarrison-Rice, J. Zou, and C. Jagadish, Growth and properties of III-V compound semiconductor heterostructure nanowires, Semicond. Sci. Technol. **26**, 014035 (2011).

[7] M. Tchernycheva, G. E. Cirlin, G. Patriarche, L. Travers, V. Zwiller, U. Perinetti, and J.-C. Harmand, Growth and characterization of InP nanowires with InAsP insertions, Nano Lett. **7**, 1500 (2007).

[8] F. Limbach, T. Gotschke, T. Stoica, R. Calarco, E. Sutter, J. Ciston, R. Cusco, L. Artus, S. Kremling, S. Höfling *et al.*, Structural and optical properties of InGaN-GaN nanowire heterostructures grown by molecular beam epitaxy, J. Appl. Phys. **109**, 014309 (2011).

[9] M. T. Björk, B. J. Ohlsson, T. Sass, A. I. Persson, C. Thelander, M. H. Magnusson, K. Deppert, L. R. Wallenberg, and L. Samuelson, One-dimensional heterostructures in semiconductor nanowhiskers, Appl. Phys. Lett. **80**, 1058 (2002).

[10] A. Nie, J. Liu, Q. Li, Y. Cheng, C. Dong, W. Zhou, P. Wang, Q. Wang, Y. Yang, Y. Zhu *et al.*, Epitaxial TiO_2/SnO_2 core-shell heterostructure by atomic layer deposition, J. Mater. Chem. **22**, 10665 (2012).

[11] S. Park, H. Ko, S. Kim, and C. Lee, Role of the interfaces in multiple networked one-dimensional core-shell nanostructured gas sensors, ACS Appl. Mater. Interfaces **6**, 9595 (2014).

[12] L. Pan, K.-K. Lew, J. M. Redwing, and E. C. Dickey, Stranski-Krastanow growth of germanium on silicon nanowires, Nano Lett. **5**, 1081 (2005).

[13] H.-J. Choi, J. C. Johnson, R. He, S.-K. Lee, F. Kim, P. Pauzauskie, J. Goldberger, R. J. Saykally, and P. Yang, Self-organized GaN quantum wire UV lasers, J. Phys. Chem. B **107**, 8721 (2003).

[14] F. Qian, Y. Li, S. Gradecak, D. Wang, C. J. Barrelet, and C. M. Lieber, Gallium nitride-based nanowire radial heterostructures for nanophotonics, Nano Lett. **4**, 1975 (2004).

[15] F. Qian, S. Gradecak, Y. Li, C.-Y. Wen, and C. M. Lieber, Core/multishell nanowire heterostructures as multicolor, high-efficiency light-emitting diodes, Nano Lett. **5**, 2287 (2005).

[16] E. Uccelli, J. Arbiol, J. R. Morante, and A. Fontcuberta i Morral, InAs quantum dot arrays decorating the facets of gaas nanowires, ACS Nano **4**, 5985 (2010).

[17] X. Jiang, Q. Xiong, S. Nam, F. Qian, Y. Li, and C. M. Lieber, InAs/InP radial nanowire heterostructures as high electron mobility devices, Nano Lett. **7**, 3214 (2007).

[18] S. Roddaro, A. Fuhrer, P. Brusheim, C. Fasth, H. Q. Xu, and L. Samuelson, Spin States of Holes in Ge/Si Nanowire Quantum Dots, Phys. Rev. Lett. **101**, 186802 (2008).

[19] R. Macêdo, J. Costa e Silva, A. Chaves, G. A. Farias, and R. Ferreira, Magnetic field induced shell-to-core confinement transition in type-II semiconductor quantum wires, J. Appl. Phys. **113**, 153710 (2013).

[20] B.-M. Nguyen, Y. Taur, S. T. Picraux, and S. A. Dayeh, Diameter-independent hole mobility in Ge/Si core/shell nanowire field effect transistors, Nano Lett. **14**, 585 (2014).

[21] H. Shu, D. Cao, P. Liang, X. Chen, and W. Lu, Band-offset effect on localization of carriers and p-type doping of InAs/GaAs core-shell nanowires, Phys. Lett. A **377**, 1464 (2013).

[22] H. Wang, M. Upmanyu, and C. V. Ciobanu, Morphology of epitaxial core-shell nanowires, Nano Lett. **8**, 4305 (2008).

[23] V. Schmidt, P. C. McIntyre, and U. Gösele, Morphological instability of misfit-strained core-shell nanowires, Phys. Rev. B **77**, 235302 (2008).

[24] S. Kwon, Z. C. Y. Chen, J.-H. Kim, and J. Xiang, Misfit-guided self-organization of anticorrelated ge quantum dot arrays on si nanowires, Nano Lett. **12**, 4757 (2012).

[25] Y. Y. Cao, G. Ouyang, C. X. Wang, and G. W. Yang, Physical mechanism of surface roughening of the radial ge-core/si-shell nanowire heterostructure and thermodynamic prediction of surface stability of the InAs-core/GaAs-shell nanowire structure, Nano Lett. **13**, 436 (2013).

[26] X. L. Li and G. W. Yang, Strain self-releasing mechanism in heteroepitaxy on nanowires, J. Phys. Chem. C **113**, 12402 (2009).

[27] V. A. Shchukin, D. Bimberg, T. P. Munt, and D. E. Jesson, Elastic interaction and self-relaxation energies of coherently strained conical islands, Phys. Rev. B **70**, 085416 (2004).

[28] X. L. Li and G. W. Yang, Theoretical determination of contact angle in quantum dot self-assembly, Appl. Phys. Lett. **92**, 171902 (2008).

[29] F. H. Stillinger and T. A. Weber, Computer simulation of local order in condensed phases of silicon, Phys. Rev. B **31**, 5262 (1985).

[30] S. Plimpton, Fast parallel algorithms for short-range molecular dynamics, J. Comput. Phys. **117**, 1 (1995).

[31] X. L. Li, G. Ouyang, and G. W. Yang, Thermodynamic theory of nucleation and shape transition of strained quantum dots, Phys. Rev. B **75**, 245428 (2007).

[32] G.-H. Lu, M. Cuma, and F. Liu, First-principles study of strain stabilization of Ge(105) facet on Si(001), Phys. Rev. B **72**, 125415 (2005).

[33] K. Tillmann and A. Förster, Critical dimensions for the formation of interfacial misfit dislocations of $In_{0.6}Ga_{0.4}As$ islands on GaAs(001), Thin Solid Films **368**, 93 (2000).

[34] J. J. Wortman and R. A. Evans, Young's modulus, shear modulus, and Poisson's ratio in silicon and germanium, J. Appl. Phys. **36**, 153 (1965).

[35] Yu. A. Burenkov, S. P. Nikanorov, and A. V. Stepanov, Elastic properties of germanium, Sov. Phys.-Solid State **12**, 1940 (1971).

[36] A. A. Stekolnikov, J. Furthmüller, and F. Bechstedt, Absolute surface energies of group-IV semiconductors: Dependence on orientation and reconstruction, Phys. Rev. B **65**, 115318 (2002).

[37] T. Mizuguchi, K.-I. Ikeda, F. Yoshida, H. Nakashima, and H. Abe, Evaluation of crystal orientation dependence of surface energy in silicon, J. Jpn. Inst. Met. **68**, 86 (2004).